Research Article | Vol. 27, No. 20 / 30 September 2019 / Optics Express 28879
Optics EXPRESS

Metamaterial infrared refractometer for determining broadband complex refractive index

HIBIKI KAGAMI,[1,3] TOMOHIRO AMEMIYA,[1,2,4] MAKOTO TANAKA,[1] YUNING WANG,[1] NOBUHIKO NISHIYAMA,[1,2] AND SHIGEHISA ARAI[1,2]

[1] *Department of Electrical and Electronic Engineering, Tokyo Institute of Technology, Tokyo 152-8552, Japan*
[2] *Institute of Innovative Research (IIR), Tokyo Institute of Technology, Tokyo 152-8552, Japan*
[3] *kagami.h.aa@m.titech.ac.jp*
[4] *amemiya.t.ab@m.titech.ac.jp*

Abstract: Infrared refractive index is an indispensable parameter for various fields including infrared photonics. To date, critical-angle refractometers, V-block refractometers, and spectroscopic ellipsometry have been commonly used to measure the refractive index. Although every method has an accuracy of four decimal places for the refractive index, a measurable wavelength region is limited up to about 2 μm. In this study, we demonstrated a metamaterial infrared refractometer for determining broadband complex refractive index. Using the device, a broadband (40–120 THz; wavelength 2.5–7.5 μm) and high-precision($< 5 \times 10^{-3}$) complex refractive index of polymethyl methacrylate was measured for the first time.

1. Introduction

"Infrared refractive index" is an indispensable parameter in various fields, including infrared photonics [1–4]. However, there is no accurate method to measure the infrared refractive index (refractive index) in the mid / near-infrared broad region (approximately 2–10 μm). At present, critical-angle refractometers and V-block refractometers are commonly used to measure the refractive index in the visible frequency range [5]. In addition, spectroscopic ellipsometry have been commercialized for measuring near-infrared refractive index [6–7]. Each refractive index measurement method has some advantages, and it is necessary to select an appropriate measurement method depending on the application. Although every method based on the determination of the critical angle of total reflection has an accuracy of four decimal places of the refractive index, a measurable wavelength region is limited up to approximately 2 μm because light scattering is quite large in the infrared band. A performance comparison table with conventional technologies is shown in Table 1.

In this study, we have demonstrated a metamaterial infrared refractometer (MMIR) for determining broadband complex refractive index. A schematic image of the measurement method is shown in Fig. 1. After the liquid sample to be measured is dropped on a metamaterial-loaded optical window (liquid samples to be measured include solid samples dissolved in solvent), the transmission characteristics are measured using an existing Fourier transform infrared spectrophotometer (FTIR) (for example, Spotlight 400 [8], LUMOS [9], AIM-9000 [10], etc.). The data obtained are rapidly analyzed to obtain the broadband complex refractive index (refractive index and absorption coefficient) of the sample.

Infrared refractive index measurement using a metamaterial-loaded optical window has the following advantages compared with commercially used refractometers [11–14]. Each feature is described in the following sections.

- Highly sensitive measurement of complex refractive index is possible in ultra-wide band from the near- to mid-infrared region.

#370661 https://doi.org/10.1364/OE.27.028879
Journal © 2019 Received 21 Jun 2019; revised 20 Aug 2019; accepted 28 Aug 2019; published 24 Sep 2019

Optics EXPRESS

Table 1. Performance comparison of various refractometers.

	Minimum argument method [11]	Abbe [12]	V-block [13]	Spectroscopic ellipsometer [14]	MMIR
Measurement wavelength range	Narrow 404.7 –2500 nm	Narrow 435.8 –643.9 nm	Wide 587.6 –1550 nm	Wide 190 –2100nm	Super wide 1300 nm –20 μm†
Sample amount	Small sample impossible	small amount (Thickness Over 10μm)	small amount (Thickness over1mm)	Extremely small amount (Thickness over 0.1nm)	A drop (Thickness over 100nm)
Sample state	solid▪ liquid	solid▪ liquid	solid▪ liquid	solid▪ liquid	liquid‡
Measurement accuracy	~1×10^{-5}	~1×10^{-4}	~2×10^{-5}	~5×10^{-3}	~5×10^{-3}
Remarks	Real part of refractive index	Real part of refractive index	Real part of refractive index	Complex refractive index	Complex refractive index

† In the MMIR, the measurement wavelength range on the short-wavelength side is limited by fabrication limit (i.e. size limit) of the metamaterial (On the other hand, the measurement wavelength range on the long-wavelength side is determined by the measurement limit of the Fourier transform infrared spectrometer)[35].
‡ Also included are solids that can be coated on to the metamaterial-loaded optical window in solution.

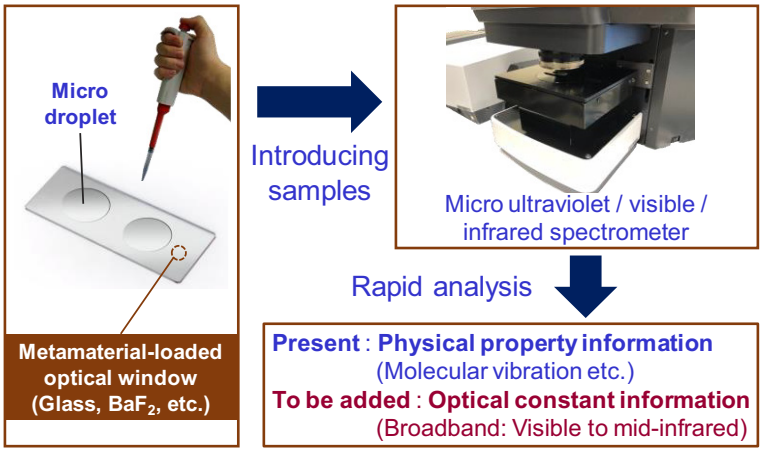

Fig. 1. Concept of metamaterial infrared refractometer for detecting broadband complex refractive index of liquid material.

- Accurate measurement can be realized even if the sample is extremely small (measurable using a single droplet of liquid sample)

The concept of the MMIR is described in Section 2, and the theoretical analysis of the metamaterial-loaded optical window to be used in the experiment is described in Section 3. Finally, using the developed MMIR, the broadband (40–120 THz; wavelength 2.5–7.5 μm) and high-precision complex refractive index of polymethyl methacrylate (PMMA) was measured for the first time (Section 4).

Optics EXPRESS

2. Refractive index measurement method using optical metamaterials

2.1. Outline of measurement method

Unlike critical-angle refractometers and V-block refractometers, the proposed measurement method derives the refractive index from the frequency response of the electromagnetic wave transmitted through the metamaterial-loaded optical window.

The MMIR has an infrared transparent BaF_2 optical window with various metamaterial arrays resonating at a specific frequency (see Fig. 2). The number of array regions 50 or more, but only nine arrays are shown in Fig. 2. Here, the resonance frequency of each region changed gradually on changing the shape of the metamaterial. In this study, we used the standard C-shaped split ring resonator (SRR) array [15–20] as the metamaterial. Although the Q factor of C-shaped SRR is not high, the resonance frequency can be represented by a form similar to the analytical solution because an individual SRR mimics a simple RLC circuit. The above features make it easy to initialize MMIR (see Section 3 for details).

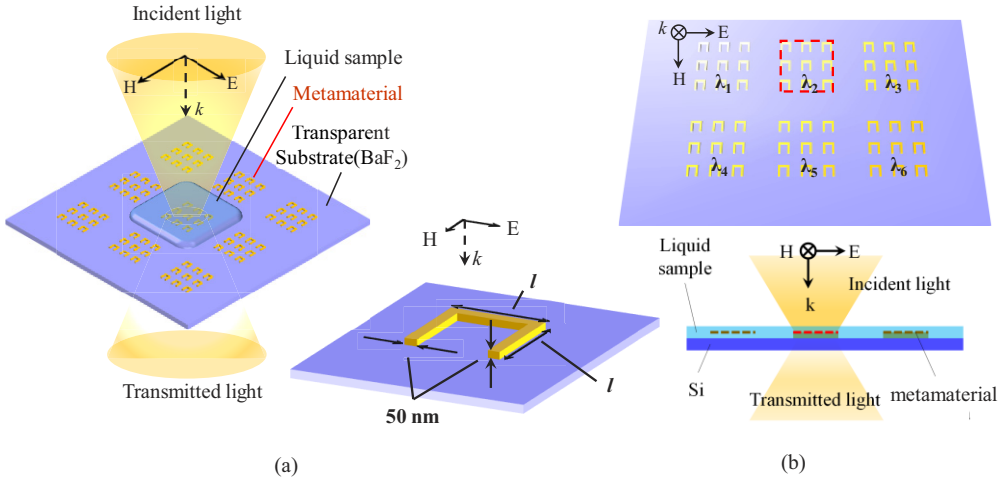

Fig. 2. Schematic of infrared refractometer using BaF_2 optical window with various metamaterial arrays.

The incident light transmission spectrum of each region is measured using an existing FTIR microscope (Shimadzu AIM-9000), as shown in Fig. 2(b). Generally, if the incident light has a frequency close to the resonance frequency, magnetic interactions occur between the light and metamaterials. When the filling metamaterial is surrounded with an appropriate liquid sample, metamaterial response changes depending on the complex refractive index (i.e., refractive index and absorption coefficient) of the sample. In particular, the following changes are observed in the transmission spectrum of the incident light.

(i) Frequency shift

A shift of energy attenuation frequency accompanying the resonance of metamaterials, which is dominated by the refractive index of the liquid sample in the vicinity of the target frequency.

(ii) Intensity change

A change in energy attenuation accompanying the resonance of metamaterials, which is dominated by the absorption coefficient of the liquid sample in the vicinity of the target frequency.

Optics EXPRESS

2.2. Measurement process

As stated in Section 2.1, we first prepare a BaF_2 optical window with various metamaterial arrays resonating at a specific frequency. The procedure for measuring the infrared refractive index by using this chip is as follows:

A. We determine the resonant frequency ω_1 of the metamaterial-loaded BaF_2 optical window through FTIR spectroscopy, corresponding to the frequency at which the transmission intensity is minimum (Fig. 3(a)).

B. A characteristic equation* of the metamaterial-loaded BaF_2 optical window (i.e., the refractive index around the metamaterial versus the resonant frequency) is determined from the results (Fig. 3(b)).

*The characteristic equation is formulated by setting the resonance frequency and the refractive index around the metamaterial as a parameter of a function. The parameters are derived from the results of finite element analysis of metamaterials of various sizes. The optical antenna is initialized in accordance with steps A and B. Then, the influence of the manufacturing error can be eliminated. Details are shown in section 3.2.

C. The liquid sample to be measured is dropped on the BaF_2 optical window and a similar measurement is performed to determine the resonance frequency ω of the metamaterial (Fig. 3(c)).

D. By comparing the obtained resonance frequency ω with the characteristic equation derived in step B, it is possible to estimate the refractive index of a measuring sample at a specific frequency (Fig. 3(d)).

E. The broadband infrared refractive index of the sample can be obtained by repeating the procedures from A to D for all antenna arrays. Finally, the broadband absorption coefficient can be derived by applying Kramers–Kronig relations [21] to the obtained refractive index profile (Fig. 3(e)).

By using the above algorithm, the MMIR can obtain an accurate broadband complex refractive index in a short time as compared with other plasmonic or metamaterial refractive index sensors [22–29].

3. Derivation of metamaterial-loaded transmission window used in MMIR

A procedure to measure the infrared complex refractive index using the MMIR is shown in Section 2.2. This procedure requires characteristic equations of the metamaterial-loaded BaF_2 window for device initialization. In this section, we derive the approximate characteristic equations used for the MMIR.

3.1. Analysis model of metamaterial-loaded transmission window

The transmission characteristics of the metamaterial-loaded BaF_2 window, which is shown in Fig. 2, were estimated using COMSOL Multiphysics based on the finite element method (FEM) [30]. In the simulation, we calculated the electromagnetic field over a cubic unit cell consisting of one gold C-ring array and measured the liquid sample on the BaF_2 substrate. A unit cell (calculation area including the minimum constituent element) was set to twice the length of the dimensional parameters l (for l, see Fig. 2) of the C ring in the x and y directions and 400 nm in the z direction (BaF_2: 200 nm, measuring liquid sample: 200 nm). The conductivity of gold was defined using the Drude model with the scattering frequency of the bulk metal [31]. In the unit cell, the Perfect Electric Conductor (PEC) boundary condition was set on the plane perpendicular

Optics EXPRESS

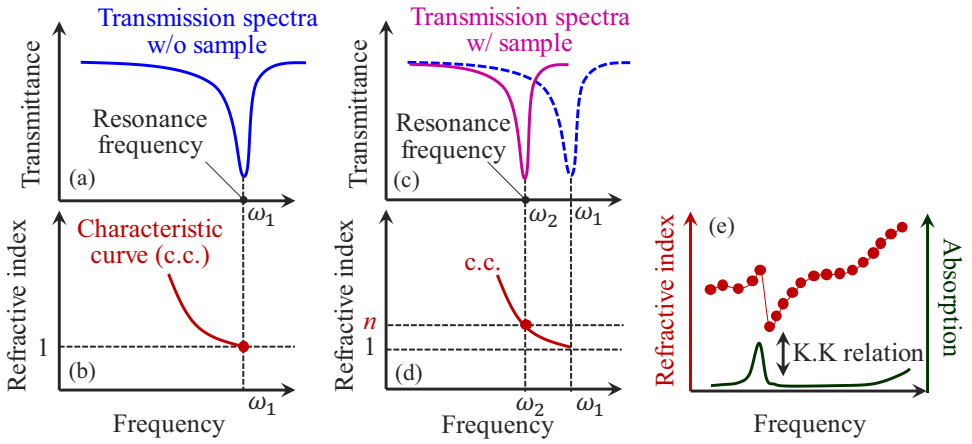

Fig. 3. Procedure of metamaterial infrared refractometer. Transmittance spectrum and characteristic curve (a)(b) w/o and (c)(d) w/ sample to be measured. (e) Broadband complex refractive index of the sample.

to the incident electric field, and the Perfect Magnetic Conductor (PMC) boundary condition was set on the plane perpendicular to the incident magnetic field.

Figure 4 shows an example of the simulated transmission spectra of liquid samples on the metamaterial-loaded BaF_2 window, when the polarization direction of the excitation light is perpendicular to the gap. In this simulation, we took the ratio of the transmission intensity of liquid samples on the BaF_2 windows w/ and w/o metamaterials. This condition was similar to that used in the measurement. As shown in Fig. 4(a), the transmission intensity varies with the magnitude of *LC* resonance and is minimum at the resonance frequency. The resonance frequency decreases with an increase in the refractive index of the liquid sample. On the other hand, as shown in Fig. 4(b), the transmission spectra exhibited stronger and sharper resonance with a decrease in the absorption coefficient of the liquid sample. From the above discussion, as the resonance frequency shift caused by the absorption coefficient of the liquid sample is extremely small, the refractive index of the liquid sample can be derived by observing a change in the resonance frequency.

We changed the dimensional parameter l of the C ring by 2 nm (For l, see Fig. 2) and made a characteristic table that shows the refractive index of the measuring liquid sample as a function of the resonance frequency. Figure 5 shows some of the results, where the value of l of the C ring varies from 150–600 nm in increments of 50 nm. According to these data, we determine an approximate characteristic equation.

3.2. Derivation of characteristic equation

The characteristic equation $\omega(n)$ for the initialization of MMIR must be an approximate expression that passes through all points in the accurate characteristic table shown in Section 3.1.

As described in Section 2.3, in this study, we used a standard C-ring metamaterial to which the *RLC* circuit model is easy to adapt. The resonance frequency of the C-ring metamaterial can be expressed in the form $\omega = 1/\sqrt{a\varepsilon}$ [32], where a is a constant and ε is the dielectric constant around the ring. Because the material around the ring is composed of the measuring liquid sample and BaF_2, the resonance frequency ε can be given by the following equation:

$$\omega = 1/\sqrt{A\varepsilon + B\varepsilon_{BaF_2}} = 1/\sqrt{An^2 + Bn_{BaF2}{}^2}, \tag{1}$$

Optics EXPRESS

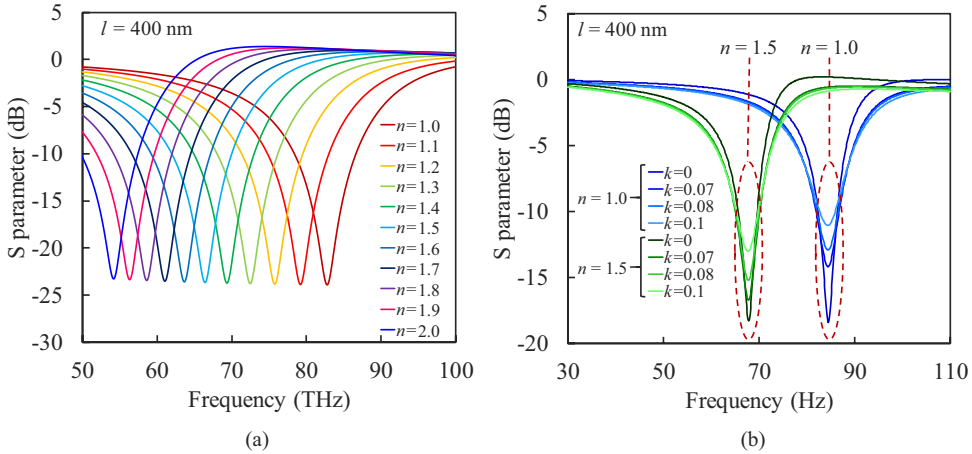

Fig. 4. One example of simulated transmission spectra of liquid samples on the metamaterial-loaded BaF_2 window, when the polarization direction of the excitation light is perpendicular to the gap. (a) Refractive index of measuring liquid sample is a parameter. (b) Absorption coefficient of measuring liquid sample is a parameter.

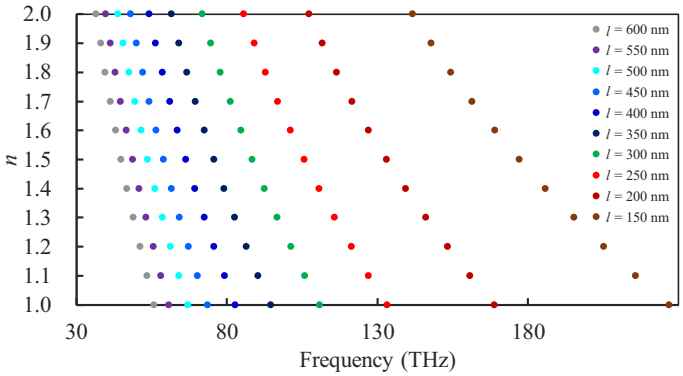

Fig. 5. Characteristic data that shows the refractive index of measuring liquid sample as a function of the resonance frequency, where l of the C ring is in the ranges of 150–600 nm in increments of 50 nm.

where ε and ε_{BaF2} are the dielectric constants of the measuring liquid sample and BaF_2, respectively. n and n_{BaF2} are the refractive indices of the measuring liquid sample and BaF_2, respectively.

In the initialization process described in Section 2.2, the characteristic equation $\omega(n)$ of the metamaterial-loaded BaF_2 window must be derived only with the resonance frequency ω_1 in air (see Fig. 3(b)). In other words, A and B in Eq. (1) need to be functions dependent only on ω_1. Considering the above, the approximate characteristic equation $\omega(n)$ should be given by the following form:

$$\omega(n) = 1/\sqrt{A(\omega_1)n^2 + B(\omega_1){n_{BaF2}}^2}, \tag{2}$$

Using Eq. (2) and the literature value of n_{BaF_2} [33], the approximate characteristic equation $\omega(n)$ was derived by machine leaning fitting with the accurate characteristic table shown in Section 3.1. As a result, $A(\omega_1)$ and $B(\omega_1)$ are given by

$$A(\omega_1) = 0.040{\omega_1}^{-1.925}, \tag{3}$$

Optics EXPRESS

$$B(\omega_1) = 1.970{\omega_1}^{-2.063}. \tag{4}$$

The characteristic equation $\omega(n)$ can be obtained by substituting the resonant frequency of the metamaterial array w/o PMMA for ω_1 in Eqs. (2)–(4). As shown in Fig. 6, it was found that the curves represented by the characteristic equation passed through all the plots calculated by the FEM.

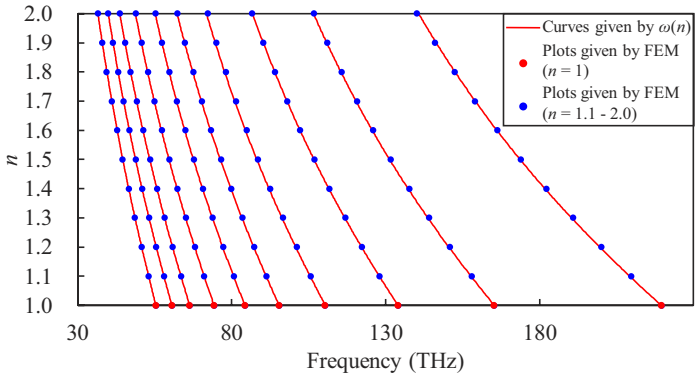

Fig. 6. Comparison of the curve derived by characteristic equation $\omega(n)$ and the accurate data calculated by the FEM.

We investigated the errors between the refractive index $n_{cc}(\omega)$ of the measuring sample derived by the characteristic equation $\omega(n)$ and the accurate refractive index $n_{FEM}(\omega)$ calculated by the FEM. The error Δn can be given by

$$\Delta n = n_{cc} - n_{FEM} = \sqrt{\left(\frac{1}{\omega^2} - B(\omega_1)\right)\frac{1}{A(\omega_1)}} - n_{FEM}(\omega). \tag{5}$$

Figure 7 shows the color plot of the result $|\Delta n|$. The dimensional parameter l of the C ring was varied from 150 nm to 600 nm in increments of 2 nm. As shown in Fig. 7, it was found that the average error was 2.649×10^{-3}. In addition, errors were within 1.5% compared with the accurate

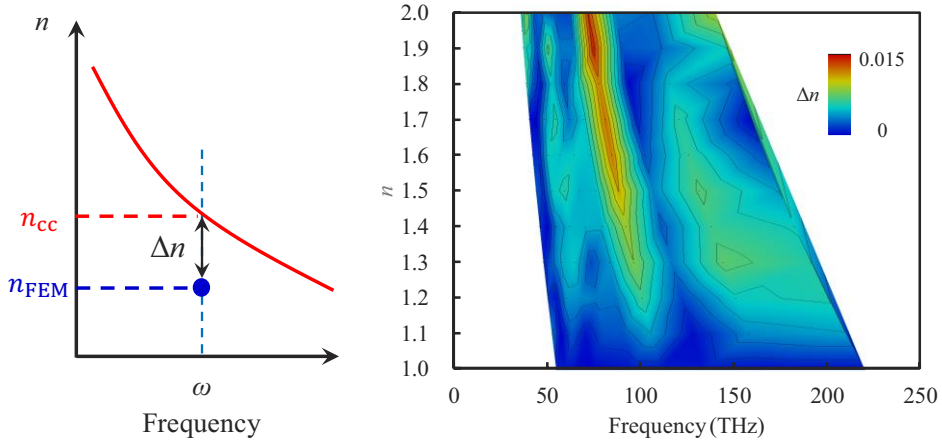

Fig. 7. Comparison of errors between the accurate characteristic curve (i.e., the refractive index around the metamaterial versus the resonant frequency) calculated by FEM and the approximate curve derived from an RLC circuit model.

Optics EXPRESS

results calculated by FEM, which means that the sensitivity of this measurement method is less than 1.5%.

4. Derivation of refractive index and absorption coefficient using PMMA

The developed MMIR was applied to PMMA, and we derive the complex infrared refractive index of PMMA from 40 to 120 THz.

4.1. Fabrication of metamaterial-loaded transmission window

A metamaterial-loaded transmission window for the MMIR was prepared initially. To fabricate the metamaterial-loaded transmission window, an infrared transparent BaF_2 wafer (φ 20 × 0.5 mm) was used as a starting substrate. After that, a PMMA resist layer with charge-dissipating agent was first spin-coated onto the BaF_2 wafer. Following spin coating, electron beam lithography (EBL) was used to deposit the desired ring array pattern onto the resist. Thereafter, a Ti layer (10 nm thickness) and an Au layer (40 nm thickness) were deposited by using electron beam deposition. Finally, a ring array comprising the Ti–Au bilayer was developed using a lift-off process.

Figure 8 shows the optical microscope image of the metamaterial-loaded transmission window fabricated with the above process, where more than 50 array regions with different resonance frequencies were prepared on the same BaF_2 wafer (nine array areas of those can be seen in Fig. 8). Figure 9 shows the scanning electron microscope (SEM) images of a specific area of the 200×200 nm C-ring array. The dimensions of the individual C-ring were designed to address the fundamental aspects of the resonance frequency shift at infrared frequencies. In this study, the dimensional parameters l of the C ring were in the ranges of 150–600 nm in increments of 50 nm, and the ring width a was fixed at 30 nm (for l, w, and a, see Fig. 2). Introducing the above metamaterial-loaded transmission window to the MMIR, the complex infrared refractive index of PMMA was measured.

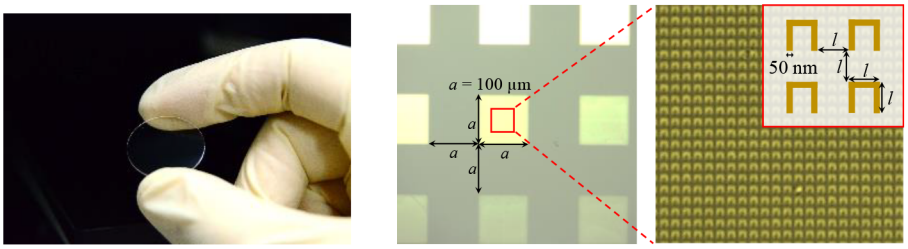

Fig. 8. Optical microscope image of metamaterial-loaded transmission window.

4.2. Complex infrared refractive index measurement of PMMA

We measured the complex infrared refractive index of PMMA with the MMIR consisting of conventional Fourier transform infrared spectrometer (IRTracer-100 and AIM-9000, Shimadzu Corp.) and the prepared metamaterial-loaded transmission window. In this study, we used a PMMA resist consisting of the polymer itself dissolved in anisole (4% in anisole). After coating metamaterial-loaded transmission window with the PMMA resist, the anisole was removed by baking process.

An example of the transmission spectra of the metamaterial-loaded transmission window with 360×360 nm C-ring arrays is shown in Fig. 10(a). In this measurement, to clarify the effect of interaction, we took the ratio of the transmission intensity of the experimental device (with

Optics EXPRESS

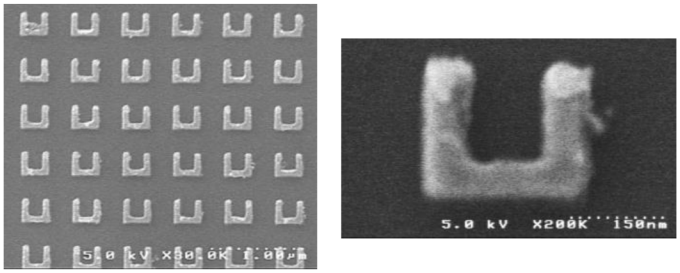

Fig. 9. Scanning electron microscope images of the 200×200-nm C-ring array in a specific area of metamaterial-loaded transmission window.

C-ring array) and that of the control device (without C-ring array). For incident light with an electric field vector perpendicular to the SRR gap, the transmission minima for the *LC* resonance is observed in the infrared range.

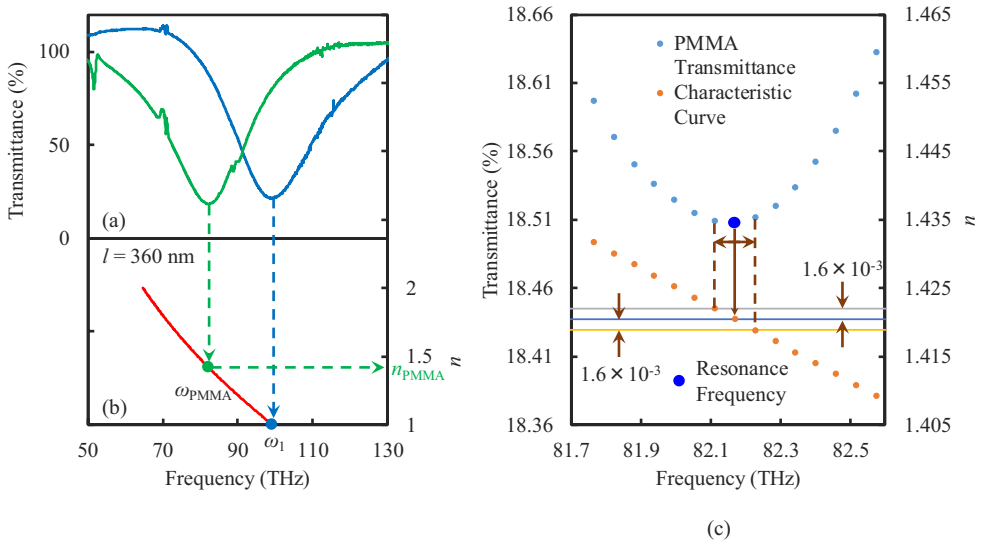

Fig. 10. (a) One example of the transmission spectra of the metamaterial-loaded transmission window with 360×360-nm C-ring arrays. (b) Refractive index of the measuring liquid sample as a function of the resonance frequency induced by the characteristic equation. (c) Enlarged view of Figs. 10(a) and 10(b) near the resonance frequency.

When PMMA was coated on the metamaterial-loaded transmission window, a clear red shift of the resonance caused by the change in the refractive index is observed, which is consistent with what we confirmed in the simulation described in Section 3. With the transmission data obtained from each metamaterial array, the refractive index of PMMA at a specific frequency was derived according to the steps A-D described in Section 2.2. Specifically, the refractive index of PMMA at a specific frequency was obtained by substituting the resonant frequencies of the C ring w/o and w/ PMMA for ω_1 and $\omega(n)$ in Eq. (1), respectively. One example is shown in Figs. 10(b). As a result, the refractive index of PMMA at a frequency of 82.16 THz was derived to be 1.420. The broadband complex refractive index of PMMA was obtained by repeating the above procedures for all metamaterial arrays. The graph that appears to be linear in Fig. 10(a) is actually a collection of plots for each measurement frequency. Therefore, the vicinity of the resonance frequency ($\omega(n)$) of the green line (w/ PMMA) in Fig. 10(a) is

Optics EXPRESS

enlarged as shown in Fig. 10(c). The resonant frequency lies between the adjacent data plots because it is monotonically decreasing / increasing up to the resonant frequency. When the frequency difference with the adjacent plot is replaced with the refractive index difference in the characteristic curve, $\Delta n = 1.6\times10^{-3}$, and the measurement error falls within this range. For all the plots shown after this, the maximum value of Δn is 2.9×10^{-3}. The accuracy of the MMIR is finally determined by the frequency resolution of the spectrometer (a higher Q factor of C-shaped SRR is also desirable, but at present stage it seems to be sufficient as can be seen from Fig. 10). Figure 6 suggests that higher measurement accuracy is required at lower frequencies. However, as shown in Fig. 10(c), the frequency resolution of the spectrometer is sufficient even when measuring on the low-frequency side. Therefore, the above fact is not problematic.

Using the broadband infrared refractive index of PMMA obtained by the method as described above, the broadband absorption coefficient was derived using Kramers–Kronig transformation. Figure 11(a) shows the frequency dependence of the complex refractive index of PMMA measured using the MMIR. As a result, we succeeded in obtaining the complex refractive index of PMMA from 40 to 120 THz (the literature value of the refractive index of PMMA from 180 THz or more is shown in [34]).

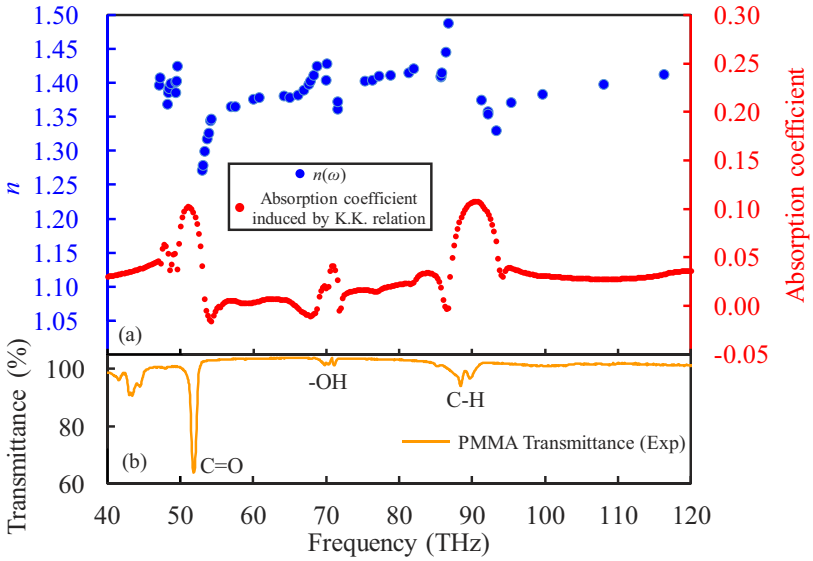

Fig. 11. Frequency dependence of the complex refractive index of PMMA measured by MMIR. The absorption spectrum measured by FTIR is also shown.

In general, it is known that the complex refractive index is largely fluctuated in the vicinity of a frequency where molecular vibration occurs. Comparing the absorption spectrum measured by FTIR spectroscopy (see Fig. 11(b)), it was confirmed that the complex refractive index fluctuated in the absorption region accompanying molecular vibration. In particular, it was found that the refractive index fluctuated at frequencies of 55 THz and 75 THz where C = O and C-H vibrations were excited.

5. Conclusion

'Infrared refractive index' is an indispensable parameter in various fields, including infrared photonics. Against that background, it is important to accurately know the infrared complex refractive indices of materials. However, the measurable wavelength limit of conventional

Optics EXPRESS

refractometers such as critical-angle refractometers, V-block refractometers, and spectroscopic ellipsometry are approximately 2 μm.

In this study, we developed an MMIR operating with just a single droplet of liquid sample. The device consists of a conventional FTIR spectrometer and a metamaterial-loaded BaF_2 optical window. Using the device, we succeeded in measuring broadband (40–120 THz; wavelength 2.5–7.5 μm) and high-precision ($< 5 \times 10^{-3}$) complex refractive index of PMMA for the first time. A comparison of the absorption spectrum with the refractive index of PMMA itself indicated that the obtained refractive index considerably fluctuated in the vicinity of a certain absorption frequency because of molecular vibration.

Table 1 shows performance comparison between the MMIR and other commercially used refractometers. In Table 1, the measurable wavelength range of the MMIR shows a maximum range of 1300 nm-20 μm, not the actual measurement range 2.5–7.5 μm. The measurable wavelength on the long-wavelength side is determined by the measurement limit of the Fourier transform infrared spectrometer. On the other hand, the measurable wavelength on the short-wavelength side is limited by fabrication limit (i.e. size limit) of the metamaterials. Considering the fabrication limit of C-shaped SRRs, the operating wavelength range is limited to 1300nm [35]. The measurable wavelength range on the short-wavelength side can be expanded by advances in metamaterial fabrication technology.

We have shown that refractive index measurement using metamaterials is possible over a wide band, and a complex refractive index can be obtained from detected broadband refractive index data. The results in this paper show that the range of material available for infrared photonics will be broadened, which will further advance this field.

Funding

Core Research for Evolutional Science and Technology (JPMJCR15N6, JPMJCR18T4); Japan Society for the Promotion of Science (#19H02193); Ministry of Internal Affairs and Communications (#182103111).

References

1. G. L. Carr, M. C. Martin, W. R. McKinney, K. Jordan, G. R. Neil, and G. P. Williams, "High-power terahertz radiation from relativistic electrons," Nature **420**(6912), 153–156 (2002).
2. R. Soref, "Mid-infrared photonics in silicon and germanium," Nat. Photonics **4**(8), 495–497 (2010).
3. B. Jalali, "Silicon Photonics: Nonlinear optics in the mid-infrared," Nat. Photonics **4**(8), 506–508 (2010).
4. T. T. Luu, M. Garg, S. Y. Kruchinin, A. Moulet, M. T. Hassan, and E. Goulielmakis, "Extreme ultraviolet high-harmonic spectroscopy of solids," Nature **521**(7553), 498–502 (2015).
5. E. C. Rhodes, "Reducing observations by the method of minimum deviations," Philos. Mag. **9**(60), 974–992 (1930).
6. D. E. Aspnes, J. B. Theeten, and F. Hottier, "Investigation of effective-medium models of microscopic surface roughness by spectroscopic ellipsometry," Phys. Rev. B **20**(8), 3292–3302 (1979).
7. G. Yu, G. Wang, H. Ichikawa, M. Umeno, T. Soga, T. Egawa, J. Watanabe, and T. Jimbo, "Optical properties of wurtzite structure GaN on sapphire around fundamental absorption edge (0.78–4.77 eV) by spectroscopic ellipsometry and the optical transmission method," Appl. Phys. Lett. **70**(24), 3209–3211 (1997).
8. Perkin Elmer, "Spotlight400," http://www.perkinelmer.co.jp/ft/tabid/596/Default.aspx
9. BRUKER, "LUMOS FTIR Microscope," https://www.bruker.com/tw/products/infrared-near-infrared-and-raman-spectroscopy/ft-ir-routine-spectrometers/lumos/overview.html.
10. SHIMADZU, "AIM-9000," https://www.shimadzu.com/an/molecular_spectro/ftir/aim/index.html.
11. SHIMADZU, "GMR-1D," https://www.shimadzu.com/opt/products/spectro/o-k25cur0000007euo.html
12. SHIMADZU, "KPR-30," https://www.shimadzu.com/opt/products/ref/o-k25cur0000007nbc.html
13. SHIMADZU, "KPR-3000," https://www.shimadzu.co.jp/products/opt/products/ref/kpr3000_01.html
14. HORIBA, "UVISEL2," https://www.horiba.com/en_en/products/detail/action/show/Product/uvisel-2-1100
15. C.-Y. Chen, I.-W. Un, N.-H. Tai, and T.-J. Yen, "Asymmetric coupling between subradiant and superradiant plasmonic resonances and its enhanced sensing performance," Opt. Express **17**(17), 15372–15380 (2009).
16. M. Decker, R. Zhao, C. M. Soukoulis, S. Linden, and M. Wegener, "Twisted split-ring-resonator photonic metamaterial with huge optical activity," Opt. Lett. **35**(10), 1593–1595 (2010).
17. T. Amemiya, T. Shindo, D. Takahashi, N. Nishiyama, and S. Arai, "Magnetic interactions at optical frequencies in an InP-based waveguide device with metamaterial," IEEE J. Quantum Electron. **47**(5), 736–744 (2011).

Optics EXPRESS

18. T. Amemiya, T. Shindo, D. Takahashi, S. Myoga, N. Nishiyama, and S. Arai, "Nonunity permeability in metamaterial-based GaInAsP/InP multimode interferometers," Opt. Lett. **36**(12), 2327–2329 (2011).
19. T. Amemiya, T. Kanazawa, S. Yamasaki, and S. Arai, "Metamaterial waveguide devices for integrated optics," Materials **10**(9), 1037 (2017).
20. S. Yamasaki, T. Amemiya, Z. Gu, J. Suzuki, N. Nishiyama, and S. Arai, "Analysis of the slow-light effect in silicon wire waveguides with metamaterials," J. Opt. Soc. Am. B **35**(4), 797–804 (2018).
21. J. S. Toll, "Causality and the dispersion relation: logical foundations," Phys. Rev. **104**(6), 1760–1770 (1956).
22. Z.-G. Dong, H. Liu, J.-X. Cao, T. Li, S.-M. Wang, S.-N. Zhu, and X. Zhang, "Enhanced sensing performance by the plasmonic analog of electromagnetically induced transparency in active metamaterials," Appl. Phys. Lett. **97**(11), 114101 (2010).
23. I. M. Pryce, Y. A. Kelaita, K. Aydin, and H. A. Atwater, "Compliant metamaterials for resonantly enhanced infrared absorption spectroscopy and refractive index sensing for refractive index sensing applications," ACS Nano **5**(10), 8167–8174 (2011).
24. X. J. He, L. Wang, J. M. Wang, X. H. Tian, J.-X. Jiang, and Z. X. Geng, "Electromagnetically induced transparency in planar complementary metamaterial for refractive index sensing applications," J. Phys. D: Appl. Phys. **46**(36), 365302 (2013).
25. D. Wu, Y. M. Liu, L. Yu, Z. Y. Yu, L. Chen, R. F. Li, R. Ma, C. Liu, J. Q. Zhang, and H. Ye, "Plasmonic metamaterial for electromagnetically induced transparency analogue and ultrahigh figure of merit sensor," Sci. Rep. **7**(1), 45210 (2017).
26. Z. R. Tu, D. S. Gao, M. L. Zhang, and D. M. Zhang, "High-sensitivity complex refractive index sensing based on Fano resonance in the subwavelength grating waveguide micro-ring resonator," Opt. Express **25**(17), 20911–20922 (2017).
27. A. Sadeqi, H. R. Nejad, and S. Sonkusale, "Low-cost metamaterial-on-paper chemical sensor," Opt. Express **25**(14), 16092–16100 (2017).
28. W. Wang, F. P. Yan, S. Y. Tan, L. N. Zhang, Z. Y. Bai, D. Cheng, H. Zhou, and Y. F. Hou, "Simultaneous measurement of refractive index and conductivity based on metamaterial absorber," J. Opt. **19**(11), 115105 (2017).
29. T. Amemiya, S. Yamasaki, M. Tanaka, H. Kagami, K. Masuda, N. Nishiyama, and S. Arai, "Demonstration of slow-light effect in siliconwire waveguides combined with metamaterials," Opt. Lett. **27**(10), 15007–15017 (2019).
30. M. J. Turner, R. W. Clough, H. C. Martin, and L. J. Topp, "Stiffness and deflection analysis of complex structures," J. Aeronaut. Sci. **23**(9), 805–823 (1956).
31. P. Drude, "Zur Elektronentheorie der Metalle," Ann. Phys. **306**(3), 566–613 (1900).
32. J. Zhou, T. H. Koschny, M. Kafesaki, E. N. Economou, J. B. Pendry, and C. M. Soukoulis, "Saturation of the magnetic response of split-ring resonators at optical frequencies," Phys. Rev. Lett. **95**(22), 223902 (2005).
33. H. H. Li, "Refractive index of alkaline earth halides and its wavelength and temperature derivatives," J. Phys. Chem. Ref. Data **9**(1), 161–290 (1980).
34. G. Beadie, M. Brindza, R. A. Flynn, A. Rosenberg, and J. S. Shirk, "Refractive index measurements of poly(methyl methacrylate) (PMMA) from 0.4–1.6 μm," Appl. Opt. **54**(31), F139–F143 (2015).
35. T. Amemiya, S. Yamasaki, M. Tanaka, H. Kagami, K. Masuda, N. Nishiyama, and S. Arai, "Demonstration of slow-light effect in a silicon-wire waveguide with a metamaterial," Opt. Express **27**(10), 15007–15017 (2019).